Proton Affinity of SO_3

Cynthia Ann Pommerening, Steven M. Bachrach, and Lee S. Sunderlin
Department of Chemistry, Northern Illinois University, DeKalb, Illinois, USA

Collision-induced dissociation (CID) of the radical cation $H_2SO_4^+$ gives the product pairs $H_2O^+ + SO_3$ and $HO + HSO_3^+$ with a 1:3 ratio that is essentially independent of collision energy. Statistical analysis of the two channels indicates that the proton affinity of HO is 3 ± 4 kJ/mol lower than that of SO_3. This can be used to derive PA(SO_3) = 591 ± 4 kJ/mol at 0 K and 596 ± 4 kJ/mol at 298 K. Previously, Munson and Smith bracketed the proton affinity as PA(HBr) = 584 kJ/mol < PA(SO_3) < PA(CO) = 594 kJ/mol. The threshold of 152 ± 16 kJ/mol for formation of $H_2O^+ + SO_3$ indicates that the barrier to CID is small or nonexistent, in contrast to the substantial barriers to decomposition for $H_3SO_4^+$ and H_2SO_4. (J Am Soc Mass Spectrom 1999, 10, 856–861) © 1999 American Society for Mass Spectrometry

The development of extensive scales of proton affinity (PA), gas basicity (GB), and acidity (ΔH_a) values has provided a framework for the quantitative understanding of ion properties. (PA = $-\Delta H$ for addition of a proton, GB = $-\Delta G$ for addition of a proton, and $\Delta H_a = \Delta H$ for deprotonation.) The history and current status of the PA and GB scales has been reviewed recently [1]. The bulk of the measurements of these properties use equilibrium constants to determine the relative thermodynamics of a pair of compounds. Such measurements are then anchored to absolute measurements, which are available for a limited number of compounds. Some molecules are not easily compared to standard references, but can be studied by less conventional means. An excellent example is the use of the energetics of decarboxylation reactions to determine the acidities of alkanes, a technique pioneered by Graul and Squires [2].

The proton affinity of sulfur trioxide is not well known or easily predicted by comparison with other molecules. One study [3] has determined the proton affinity of SO_3 by noting that in an ion source, reaction 1 is fast (although apparently reversible), whereas the equilibrium for reaction 2 lies to the right. This suggests that the proton affinity of SO_3 lies

$$HSO_3^+ + CO \rightarrow HCO^+ + SO_3 \quad (1)$$

$$H_2Br^+ + SO_3 \rightarrow HSO_3^+ + HBr \quad (2)$$

between those of HBr (584 kJ/mol) and CO (594 kJ/mol) [1]. Interpreting the results of such studies is difficult because of the uncertain temperature and neutral concentrations in the ion source. The results from this work provide an independent measurement of the PA of SO_3.

The gas-phase addition of H_2O to SO_3 to form sulfuric acid has a substantial barrier, as indicated by reaction rate measurements [4–6] and computational results [7, 8]. A similar barrier is seen for the reaction of protonated water with SO_3 [9]. This was determined by measuring the activation barrier for the reverse reaction, collision-induced dissociation (CID) of $H_3SO_4^+$, and corroborated by further computational results. The present work explores CID of the similar molecule $H_2SO_4^+$ to determine the effect of the removal of an electron on the potential energy surface of sulfuric acid.

Experimental

The flowing afterglow tandem mass spectrometer used in these experiments consists of an ion source, a flow reactor, and a tandem mass spectrometer comprising a quadrupole mass filter, an octopole ion guide [10], a second quadrupole mass filter, and a detector. This instrument has been described in detail previously [11]; a brief description follows.

The ion source used in these experiments is a dc discharge that typically operates at 1000 V with 1 mA of emission current. The ions studied in this work were produced by addition of fuming sulfuric acid to the ion source. This produced ions of *m/z* 98 and 99, which correspond to $H_2SO_4^+$ and $H_3SO_4^+$ [9, 12]. Other ions qualitatively consistent with those seen in the electron impact ionization spectra of sulfuric acid [13] were also seen. Isotope intensity patterns were consistent with these assignments.

The flow tube is a 92 cm × 7.3 cm i.d. stainless steel pipe with five neutral reagent inlets. The buffer gas is 95% He and 5% Ar. The pressure in the flow tube is 0.4 torr and the buffer gas flow velocity is 100 m/s, giving approximately 10^5 collisions with the buffer gas to thermalize the ions. The helium flows through a molec-

Address reprint requests to Lee Sunderlin, Department of Chemistry, Northern Illinois University, DeKalb, IL 60115. E-mail: sunder@niu.edu

In memory of Robert R. Squires, mentor and friend.

1044-0305/99/$20.00
PII S1044-0305(99)00055-0

Received January 14, 1999
Revised May 10, 1999
Accepted May 10, 1999

ular sieve trap that is cooled by liquid nitrogen to remove condensible impurities. The relative ratio of $H_2SO_4^+$ and $H_3SO_4^+$ is strongly dependent on the condition of the flow tube, with wet conditions resulting in more $H_3SO_4^+$ (presumably from proton transfer) and dry conditions resulting in more $H_2SO_4^+$ (presumably from direct ionization).

Ions are sampled from the flow tube into the main chamber, which contains the tandem mass spectrometer. This chamber is differentially pumped to pressures sufficiently low that further collisions of the ions with the buffer gas are unlikely. The operating conditions for the first quadrupole were set to ensure that only ions of *m/z* 98 were allowed to pass into the octopole, which passes through a gas cell that is filled with argon for the CID experiments. The intensities of the products and unreacted ions were measured by the second quadrupole and the electron multiplier detector. The resolution of the second quadrupole was usually left low to improve collection efficiency and reduce mass discrimination. In some cases, the cross section for H_2O^+ was corrected for overlap with the peak for H_3O^+. This ion is formed by proton transfer to adventitious water in the gas cell. The cross section for this reaction declines with translational energy roughly as $E^{-1.3}$, and this interference is not significant above 2 eV (1 eV = 96.49 kJ/mol).

Threshold Analysis

The threshold energy for a reaction is determined by modeling the intensity of product ions as a function of the reactant ion kinetic energy in the center-of-mass (CM) frame, E_{CM}. The translational energy zero of the reactant ion beam is measured using the octopole as a retarding field analyzer [10, 14]. The first derivative of the beam intensity as a function of energy is approximately Gaussian, with a full-width at half-maximum of typically 1.0 eV for these experiments. A small fraction of the ions can be translationally excited in excess of this distribution by the rf fields of the first quadrupole. This results in additional tailing at the lowest energies in the cross section data. The effect of this tailing is included in the overall uncertainty in the reported reaction thresholds. The laboratory energy E_{lab} is given by the octopole rod offset voltage measured with respect to the center of the Gaussian fit. Conversion to the CM frame is accomplished by use of $E_{CM} = E_{lab}m/(m + M)$, where m and M are the masses of the neutral and ionic reactants, respectively. This energy is corrected at low offset energies to account for truncation of the ion beam [14].

Total cross sections for reaction σ_{total} are calculated using $I = I_0 \exp(-\sigma_{total}nl)$ [14], where I is the intensity of the reactant ion beam, I_0 is the intensity of the incoming ion beam ($I_0 = I + \Sigma I_i$), and I_i are the intensities for each product ion. The number density of the neutral collision gas is n, and l is the effective collision cell length, 13 ± 2 cm [11]. Individual product cross sections σ_i are equal to $\sigma_{total}(I_i/\Sigma I_i)$.

To derive CID threshold energies, the threshold region of the data is fitted to the model function given in eq 3 [14], where $\sigma(E)$ is the cross section for formation of the product ions

$$\sigma(E) = \sigma_0\Sigma_i[g_iP_D(E,E_i)(E + E_i - E_T)^n/E] \quad (3)$$

at CM energy E, E_T is the desired threshold energy, σ_0 is a scaling factor, n is an adjustable parameter, P_D is the probability of an ion with a given amount of energy dissociating within the experimental window (~30 μs), and i denotes vibrational states having energy E_i and population g_i ($\Sigma g_i = 1$). P_D and the branching fractions for multiple dissociation pathways were calculated using the RRKM formalism. The transition states were assumed to be at the centrifugal barriers, where most of the degrees of freedom are equal to those in the products. The CRUNCH program written by Armentrout and co-workers was used in this threshold analysis; the statistical modeling procedures have been extensively discussed recently [15]. Rotational energy was handled using the equipartitioning approximation [15]. The effects of the energy distribution of the ion beam, Doppler motion of the neutral target gas, and the kinetic energy distribution of the reactant ion are accounted for by the CRUNCH program.

The collision gas pressure can influence the observed cross sections because of secondary collisions. This is accounted for by linear extrapolation of data taken at several pressures to a zero pressure cross section [16].

The uncertainty in the reaction thresholds because of the internal energy of the reactant ions and kinetic shifts in the thresholds is estimated by determining the threshold with the calculated frequency sets multiplied by 0.9, 1.0, and 1.1. Also, the uncertainty in the energy scale is 0.15 eV in the lab frame. The uncertainty associated with a factor of 3 change in the 30 μs time window for dissociation is 0.001 eV. These uncertainties are combined with the standard deviation of the thresholds derived from different data sets to give the overall uncertainty in reaction energetics.

Calculations

The geometry of $H_2SO_4^+$ was optimized at the B3LYP/6-31G(*d*) level, H_2O^+ was optimized at the MP2/6-31G(*d*) level, and both HSO_3^+ and SO_3 were optimized at the HF/6-31G(*d*) level. Rotational and vibrational constants were then calculated at these levels of theory, and the vibrational constants were scaled by factors of 0.943 for MP2/6-31G(*d*) and 0.89 for HF/6-31G(*d*). The B3LYP/6-31G(*d*) results were used without scaling. The nature of the stable structures was verified by the existence of zero imaginary vibrational frequencies. All calculations were performed using GAUSSIAN-94 [17]. The frequencies used in the fitting procedure are given in Table 1.

Table 1. Molecular constants[a]

Molecule	Vibrational frequencies (cm^{-1})	Rot. constants (cm^{-1})
$H_2SO_4^+$	161, 278, 323, 358, 403, 443, 451, 785, 825, 946, 1072, 1143, 1221, 3544, 3561	0.147, 0.160, 0.178
HO	3738	18.9 (×2)
H_2O^+	1431, 3157, 3326	8.50, 12.2, 27.9
SO_3	501, 519 (×2), 1079, 1383 (×2)	0.178, 0.356 (×2)
HSO_3^+	435, 445, 484, 499, 939, 1092, 1268, 1537, 3370	0.167, 0.327, 0.344

[a]Experimentally measured parameters for OH taken from [19]. Other values calculated as discussed in text.

Because of difficulties in convergence of the HF equations and/or the geometry optimization, we decided not to further pursue the goal of obtaining the calculated frequencies for all species at the same high level of theory. Although the frequencies obtained at the MP2 and HF levels are scaled before use, further improvement in the computational level is unlikely to alter the values of the scaled frequencies appreciably. The calculated values for H_2O^+ are in good agreement with the incomplete set of experimental values [18]. Scaled HF/6-31G(*d*) frequencies for SO_3 agree well (within 2%) with the experimental values, suggesting that this level of calculation is also sufficient for HSO_3^+.

Results

The cross sections for CID of $H_2SO_4^+$ with Ar are shown in Figure 1. The major products correspond to reactions 4 and 5, formation of hydroxyl and sulfur trioxide with one of these two moieties retaining the additional proton. In addition, a small amount (~4%) of reaction 6 is seen. Figure 2 shows the branching ratio for the main products. Reasonable variations in focusing and ion collection parameters give ~20% variations in the branching ratio.

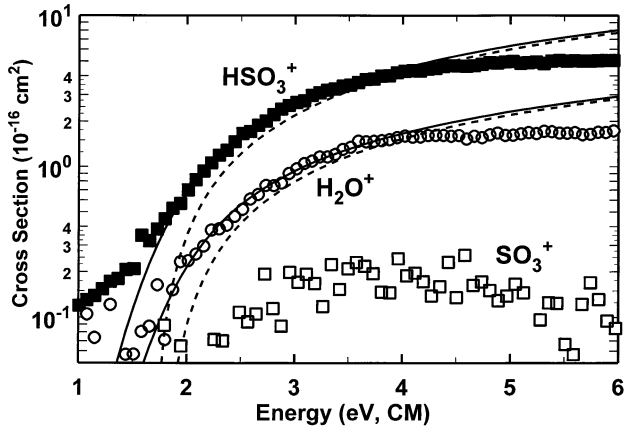

Figure 1. Appearance curves for CID of $H_2SO_4^+$ as a function of kinetic energy in the CM frame. The solid lines are convoluted fits to the data and the dashed lines are unconvoluted fits to the data. The fitting parameters for this data are $E_T(4) = 1.654$ eV, $E_T(5) = 1.690$ eV, and $n = 1.65$. See text for a discussion of the fitting parameters.

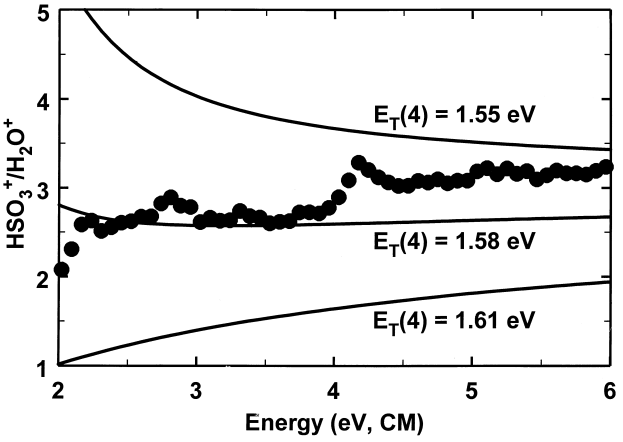

Figure 2. Branching ratio for reactions 5 and 4 as a function of energy in the CM frame. The three lines indicate predicted branching ratios assuming the threshold for reaction 5 is 1.61 eV and the threshold for reaction 4 is 1.61, 1.58, or 1.55 eV.

$$H_2SO_4^+ \rightarrow HO + HSO_3^+ \quad (4)$$

$$\rightarrow H_2O^+ + SO_3 \quad (5)$$

$$\rightarrow H_2O + SO_3^+ \quad (6)$$

The small amount of reaction 6 observed suggests that most of the reactant ions are $H_2SO_4^+$ rather than $H_2O \cdot SO_3^+$, which should undergo CID to give both SO_3^+ and H_2O^+. These two processes differ in energy by the small difference in the ionization potentials: IP(H_2O) = 12.621 eV and IP(SO_3) = 12.80 ± 0.04 eV [19].

Discussion

There are two possibilities for the dynamics of this CID reaction. One is that the dissociation is statistical, and the product branching ratio depends only on the thermodynamic properties of the reactants and products. This hypothesis will be assumed in the following discussion. The other possibility, a direct reaction with a nonstatistical product distribution, will be discussed below.

Cross Section Modeling

The best fit to the experimental data using coupled reaction channels with a statistical product distribution is shown in Figure 1. The fitting parameters used are $n = 1.6 \pm 0.2$, $E_T(4) = 1.58 \pm 0.16$ eV, and $E_T(5) = 1.61 \pm 0.16$ eV. Including uncertainties of 0.05 eV for the effect of varying the vibrational frequencies and 0.04 eV for the energy scale uncertainty in the CM frame, the threshold values are 1.58 ± 0.17 eV (152 ± 16 kJ/mol)

for reaction 4 and 1.61 ± 0.17 eV (155 ± 16 kJ/mol) for reaction 5.

Other than the rotational and vibrational frequencies, the main parameters are the polarizabilities of the neutral fragments [20], the reduced masses, and the symmetry numbers of the products. The symmetry numbers are 6 for SO_3, 2 for H_2O^+, 1 for OH, and 1 for HSO_3. The effect of symmetry is substantial because the product of symmetry numbers is 12 for the products of reaction 5 and 1 for the products of reaction 4. This favors reaction 4 by a factor of 12. The other parameters favor reaction 5 by roughly a factor of 6 at higher energies. The major influence is that the products of reaction 5 have one more rotational constant (and thus a higher density of states) than the products of reaction 4.

The threshold for reaction 4 is 36 ± 4 meV lower than the threshold for reaction 5. This difference was calculated from relative thresholds for individual data sets where both products were monitored. The error limits on this value are much smaller than for the individual thresholds because many sources of error, such as the uncertainty in the ion beam energy zero or the reactant internal energy, have a negligible effect on the *difference* between two thresholds. Fits to the data sets without pressure extrapolation give an essentially identical difference of 38 ± 4 meV, indicating that the pressure affects both cross sections equally. Substantial changes in the fitting range give variations of up to ±10 meV in the derived difference. Allowing the scaling of the two cross sections to be varied independently causes a variation of typically 10 meV, usually in the direction of a smaller difference in thresholds. Scaling the reactant frequencies does not have an effect, but scaling the frequency set for one of the products by 10% causes a variation of 22 meV. The primary effect here is that scaling one frequency set has a significant effect on the density of states for that product, which alters the predicted branching ratio. The optimized fit therefore has different relative thresholds to compensate for the different relative cross sections. Accounting for all of these potential sources of error gives a final difference of 36 ± 27 meV. Threshold analysis therefore indicates that SO_3 has a higher 0 K proton affinity than OH by 36 ± 27 meV.

Figure 2 shows the branching ratio for the products of reactions 4 and 5, as well as the predicted branching ratios assuming the threshold for reaction 5 is 1.61 eV and the threshold for reaction 4 is 0.00, 0.03, or 0.06 eV lower. Two aspects of the predicted cross sections can be compared to the experimental data: the magnitude and the shape. The magnitude of the experimental branching ratio is most consistent with an energy difference of 0.03–0.05 eV. The slight upward trend in the data matches that predicted with an energy difference of 0.00–0.03 eV. Thus, all three determinations of the difference in the thresholds for reactions 4 and 5 give very similar numbers. This leads to the conclusion that $PA(SO_3) - PA(OH) = 3 \pm 4$ kJ/mol at 0 K. The error limit reported is somewhat larger than the statistical uncertainty to account for unforeseen systematic effects.

Direct Reaction

The other possible reaction mechanism is that the product distribution is influenced by the structure of the reactant ion. Because loss of OH from $H_2SO_4^+$ is a direct reaction, whereas loss of H_2O^+ involves a rearrangement, this possibility should lead to preferentially more OH loss (the kinetically preferred product) at higher energies. Thus, if direct dissociation occurs, the amount of reaction 4 observed should be greater than predicted, and the experimental branching ratio for reactions 4 and 5 should be higher than the statistical prediction.

Some of the 15% rise in the experimental branching ratio from ~3.5 to 6 eV could be due to direct dissociation. It is also likely that collection of the lighter H_2O^+ product is somewhat less efficient at higher energies. Varying the focusing conditions causes changes in the branching ratio of this magnitude at energies above 4 eV. In either case, the agreement of all three methods of determining the difference in reaction thresholds confirms the hypothesis that the dissociation is predominantly statistical, particularly in the threshold region.

PA(SO_3)

The proton affinity of OH is needed to determine the proton affinity of SO_3. The thermochemistry in this paragraph is all for a temperature of 0 K. The ionization potential of water has been measured to be 12.6223 and 12.6188 eV [18]; these values are averaged in the NIST database [19] as $IP(H_2O) = 12.621 \pm 0.002$ eV, or 1217.7 ± 0.2 kJ/mol. This can be combined with the heat of formation of water to give $\Delta_f H(H_2O^+) = 978.8 \pm 0.2$ kJ/mol. The sum of the heats of formation for OH and H^+ is 1566.9 ± 1.2 kJ/mol, so the 0 K proton affinity of OH is 588.1 ± 1.2 kJ/mol. This value is actually more precise than that of many of the more commonly used primary PA standards. It can be combined with the difference derived above to give $PA(SO_3) = 591 \pm 4$ kJ/mol at 0 K. Finally, the frequencies given above can be used to derive $PA(SO_3) = 596 \pm 4$ kJ/mol at 298 K.

Comparison to Previous Work

The 298 K proton affinity of SO_3 was previously bracketed [3] between those for HBr (584 kJ/mol, with no uncertainty reported) and CO (594 ± 3 kJ/mol [1]. This leads to the value of 589 kJ/mol reported in the recent comprehensive review of proton affinities [1]. The lower limit is consistent with that derived in the present work. The upper limit is within the combined uncertainties of the measurements. The experimental observation that proton transfer from SO_3 to CO is "rapid" can be readily explained by noting that if the reaction is

Table 2. Literature thermochemistry[a]

Species	$\Delta_f H$ (0 K)[b]	$\Delta_f H$ (298 K)
H_2SO_4	−721.2 ± 8.4	−735.1 ± 8.4
H_2O	−238.92 ± 0.04	−241.83 ± 0.04
$HO^{\cdot}$	38.7 ± 1.2	39.0 ± 1.2
H_2O^+	978.8	
SO_3	−390.03 ± 0.71	−395.77 ± 0.71
HSO_3^+[c]	547 ± 4	538 ± 4
H^+	1528.2 ± 0.1	1530.1 ± 0.1

[a]All values for gas phase species in kJ/mol. Unless otherwise noted, values from [19].
[b]Corrections from 298 to 0 K calculated from first principles or taken from Chase, M. W., Jr.; Davies, C. A.; Downey, J. R., Jr.; Frurip, D. J.; McDonald, R. A.; Syverud, A. N. *J. Phys. Chem. Ref. Data* **1985,** *14,* Suppl. 1. (JANAF Tables).
[c]This work.

3 kJ/mol endothermic, as suggested here, the reaction can still be up to 23% efficient at room temperature. The relatively high pressure conditions used in the previous work may be more consistent with ΔG controlling the relative reaction rates rather than ΔH [21]. Using calculated entropies of protonation [22] with the experimental enthalpies of protonation, GB(CO) = 563 ± 3 kJ/mol and GB(HBr) = 558 kJ/mol. Using the frequencies calculated above, GB(SO_3) = 569 ± 4 kJ/mol. This suggests that ΔG for proton transfer from SO_3 to CO is 6 ± 5 kJ/mol. An endothermicity of 6 kJ/mol would still allow the reaction to be up to 8% efficient at room temperature.

Snow and Thomas [13] measured the following appearance potentials for ions formed from electron impact (EI) on sulfuric acid vapor at 381 K: AP(H_2O^+) = 13.2 ± 0.2 eV, AP(SO_3^+) = 13.8 ± 0.2 eV, AP($H_2SO_4^+$) = 12.40 ± 0.05 eV, and AP(HSO_3^+) = 13.90 ± 0.10 eV. Neglecting the temperature difference, the EI appearance potentials can be used with data in Table 2 to derive the thermochemistry of several of the species involved in the present work at 298 K. The first two APs can be used to derive heats of formation for the neutral precursor, $\Delta_f H(H_2SO_4)$ = −695 ± 21 kJ/mol or −703 ± 21 kJ/mol. The latter two APs can be used to derive heats of formation for products, $\Delta_f H(HSO_3^+)$ = 567 ± 13 kJ/mol, and $\Delta_f H(H_2SO_4^+)$ = 461 ± 21 kJ/mol [13]. The first pair of numbers is in moderate disagreement (by 32–40 ± 23 kJ/mol) with the 298 K value in Table 2. The second number differs from the present results by 29 ± 14 kJ/mol and from the results of Munson and co-workers [3] by 36 ± 14 kJ/mol. The third result can be used with the 298 K thermochemistry in Table 2 to predict endothermicities for reactions 4 and 5 of 116 ± 11 and 119 ± 10 kJ/mol, respectively. The measured 0 K thresholds for reactions 4 and 5 are 152 ± 16 and 155 ± 16 kJ/mol, giving discrepancies of 36 ± 19 kJ/mol for both reactions. Thus, the absolute EI appearance potentials are somewhat inconsistent with other results for these molecules.

Because the internal energy of H_2SO_4 should affect all of the EI appearance potentials in a similar way, the *differences* between the appearance potentials for the parent $H_2SO_4^+$ ion and three of the decomposition products may be more comparable to the reaction thresholds measured here. The AP difference for HSO_3^+ of 1.50 ± 0.11 eV is in very good agreement with the reaction 4 threshold of 1.58 ± 0.16 eV. The AP difference for H_2O^+ of 0.8 ± 0.2 eV is significantly lower than the reaction 5 threshold of 1.61 ± 0.16 eV, and the AP difference for SO_3^+ of 1.4 ± 0.2 eV is inconsistent with SO_3^+ being a minor product in the present work. These latter two values are complicated by interference with ionization of H_2O and SO_3, which are present along with H_2SO_4 in the source gas [13].

The PA(SO_3) value calculated at the HF/6-31G(*d*) level is 574 kJ/mol at 0 K. Although this level of theory is not very high, the derived proton affinity is in qualitative agreement with the experimental value of 591 kJ/mol.

Reaction Barriers

Reaction 4 is a spin-allowed heterolytic bond cleavage from a doublet reactant to doublet + singlet products. The geometry around the sulfur atom changes moderately from approximately tetrahedral to approximately trigonal planar. Such reactions typically do not have a barrier in ionic systems because of the ion–dipole and ion–induced dipole attractions. For example, there is no barrier to loss of hydroxide from $HOSO_2^-$ or $HOCO_2^-$, where similar geometry changes occur [23]. After the S–OH bond is broken, a loose $HSO_3^+ \cdot OH$ complex is at least transiently present. If this complex has a lifetime longer than the rotational period of HSO_3^+, then the second hydrogen will probably contact the OH group, allowing reaction 5 to occur through proton transfer. This proton transfer step, which has no significant geometry change, is very unlikely to have a barrier in excess of the ion–permanent dipole attraction. This model is consistent with the calculated RRKM dissociation rates, assuming the excess energy of the activated complex is distributed statistically among the available degrees of freedom.

A barrier to the initial hydroxyl loss should lead to the two channels having the same threshold. Instead, the two channels have a consistent difference in their thresholds. Also, if the difference in the energetics of the two channels were not 3 ± 4 kJ/mol as derived above, then the experimental branching ratio would not match the predicted results over a broad energy range.

Some of the differences between the EI results and the CID results could be explained by barriers to CID. For instance, a barrier to reaction 5 but not to reaction 4 would explain the discrepancies observed in the relative appearance potentials. However, such a barrier is inconsistent with the product branching ratios mentioned above. Furthermore, similar discrepancies of a few tenths of an electron volt are seen in the other thermochemical comparisons detailed in the previous section.

The dissociations of H_2SO_4 and $H_3SO_4^+$ have barriers of 159–167 kJ/mol [3, 7] and 224 kJ/mol [9] for loss of water and protonated water, respectively. These barriers are significantly in excess of the reaction endothermicities. Similarly, there are barriers of 210 kJ/mol and ~230 kJ/mol for water loss from H_2CO_3 [23] and $(HO)_2PO_2^-$ [24]. The difference between these reactions and dissociation of $H_2SO_4^+$ is that $H_2SO_4^+$ has an OH loss channel that is relatively low in energy. Such a reaction for H_2SO_4 or $H_3SO_4^+$ is apparently higher in energy than long-distance proton migration, which is calculated to be the lowest energy reaction path for both systems. Thus, the key difference between the dissociation dynamics of $H_2SO_4^+$ and other oxyacid species is that the radical nature of $H_2SO_4^+$ allows S–O bond cleavage to occur.

Acknowledgments

Peter Armentrout, Kent Ervin, and Mary Rodgers are thanked for developing the improved version of the CRUNCH data analysis program. Timothy Thomas and the reviewers are thanked for helpful comments on this work.

References

1. Hunter, E. P. L.; Lias, S. G. *J. Phys. Chem. Ref. Data* **1998,** *27*, 413–657.
2. Graul, S. T.; Squires, R. R. *J. Am. Chem. Soc.* **1988,** *110*, 607–608. **1989,** *111*, 892–899. **1990,** *112*, 2517–2529. Graul, S. T.; Squires, R. R. *Int. J. Mass Spectrom. Ion Processes* **1990,** *100*, 785.
3. Munson, B.; Smith, D.; Polley, C. *Int. J. Mass Spectrom. Ion Phys.* **1977,** *25*, 323–326.
4. Kolb, C. E.; Jayne, J. T.; Worsnop, D. R.; Molina, M. J.; Meads, R. F.; Viggiano, A. A. *J. Am. Chem. Soc.* **1994,** *116*, 10314–10315.
5. Jayne, J. T.; Pöschl, U.; Chen, Y.-M.; Dai, D.; Molina, L. T.; Worsnop, D. R.; Kolb, C. E.; Molina, M. J. *J. Phys. Chem.* **1997,** *101*, 10000–10011.
6. Lovejoy, E. R.; Hanson, D. R.; Huey, L. G. *J. Phys. Chem.* **1996,** *100*, 19911–19916.
7. Morokuma, K.; Muguruma, C. *J. Am. Chem. Soc.* **1994,** *116*, 10316–10317.
8. Hofmann, M.; von R. Schleyer, P. *J. Am. Chem. Soc.* **1994,** *116*, 4947–4952.
9. Pommerening, C. A.; Bachrach, S. M.; Sunderlin, L. S. *J. Phys. Chem. A* **1999,** *103*, 1214–1220.
10. Gerlich, D. *Adv. Chem. Phys.* **1992,** *82*, 1–176.
11. Do, K.; Klein, T. P.; Pommerening, C. A.; Sunderlin, L. S. *J. Am. Soc. Mass Spectrom.* **1997,** *8*, 688–696.
12. Do, K.; Klein, T. P.; Pommerening, C. A.; Bachrach, S. M.; Sunderlin, L. S. *J. Am. Chem. Soc.* **1998,** *120*, 6093–6096.
13. Snow, K. B.; Thomas, T. F. *Int. J. Mass Spectrom. Ion Processes* **1990,** *96*, 49–68.
14. Ervin, K. M.; Loh, S. K.; Aristov, N.; Armentrout, P. B. *J. Phys. Chem.* **1983,** *87*, 3593. Ervin, K. M.; Armentrout, P. B. *J. Chem. Phys.* **1985,** *83*, 166–189.
15. Rodgers, M. T.; Ervin, K. M.; Armentrout, P. B. *J. Chem. Phys.* **1997,** *106*, 4499–4508. Rodgers, M. T.; Armentrout, P. B. *J. Chem. Phys.* **1998,** *109*, 1787–1800.
16. Loh, S. K.; Hales, D. A.; Lian, L.; Armentrout, P. B. *J. Chem. Phys.* **1989,** *90*, 5466. Schultz, R. H.; Crellin, K. C.; Armentrout, P. B. *J. Am. Chem. Soc.* **1991,** *113*, 8590.
17. GAUSSIAN-94. Frisch, M. J.; Trucks, G. W.; Schlegel, H. B.; Gill, P. M. W.; Johnson, B. G.; Robb, M. A.; Cheeseman, J. R.; Keith, T.; Petersson, G. A.; Montgomery, J. A.; Raghavachari, K.; Al-Laham, M. A.; Zakrzewski, V. G.; Ortiz, J. V.; Foresman, J. B.; Cioslowski, J.; Stefanov, B. B.; Nanayakkara, A.; Challacombe, M.; Peng, C. Y.; Ayala, P. Y.; Chen, W.; Wong, M. W.; Andres, J. L.; Replogle, E. S.; Gomperts, R.; Martin, R. L.; Fox, D. L.; Binkley, J. S.; Defrees, D. J.; Baker, J.; Stewart, J. J. P.; Head-Gordon, M.; Gonzales, C.; Pople, J. A. Gaussian, Inc.: Pittsburgh, PA, 1995.
18. Reutt, J. E.; Wang, L. S.; Lee, Y. T.; Shirley, D. A. *J. Chem. Phys.* **1986,** *85*, 6928–6939. Page, R. H.; Larkin, R. J.; Shen, Y. R.; Lee, Y. T. *J. Chem. Phys.* **1988,** *88*, 2249–2263.
19. *NIST Chemistry WebBook*, NIST Standard Reference Database Number 69; Mallard, W. G.; Linstrom, P. J., Eds., November 1998 release, National Institute of Standards and Technology: Gaithersburg, MD 20899 (http://webbook.nist.gov).
20. Miller, K. J. *J. Am. Chem. Soc.* **1990,** *112*, 8533–8542.
21. Meot-ner, M. *J. Phys. Chem.* **1991,** *95*, 6580–6585.
22. East, A. L. L.; Smith, B. J.; Radom, L. *J. Am. Chem. Soc.* **1997,** *119*, 9014–9020.
23. Squires, R. R. *Int. J. Mass Spectrom. Ion Processes* **1992,** *117*, 565–600.
24. Blades, A. T.; Ho, Y.; Kebarle, P. *J. Am. Chem. Soc.* **1996,** *118*, 196–201.